

Impedance Spectroscopy Study of the Electrical Properties of Cation-Substituted Barium Hexaaluminate Ceramics

B. A. Belyaev^{a, b, *}, N. A. Drokin^{a, c}, and V. A. Poluboyarov^d

^a *Kirensky Institute of Physics, Federal Research Center KSC SB RAS, Russian Academy of Sciences, Krasnoyarsk, 660036 Russia*

^b *Siberian Federal University, Krasnoyarsk, 660041 Russia*

^c *Siberian State Aerospace University, Krasnoyarsk, 660014 Russia*

^d *Institute of Solid State Chemistry and Mechanochemistry, Siberian Branch, Russian Academy of Sciences, Krasnoyarsk, 660036 Russia*

**e-mail: belyaev@iph.krasn.ru*

Received July 12, 2017

Abstract—We report on the behavior of frequency and temperature dependences of the impedance of a measuring cell in the form of a parallel-plate capacitor filled with barium hexaaluminate ceramics with four aluminum cations replaced by iron ($\text{BaO} \cdot 2\text{Fe}_2\text{O}_3 \cdot 4\text{Al}_2\text{O}_3$). The measurements have been performed in the frequency range of $0.5\text{--}10^8$ Hz at temperatures of $20\text{--}375^\circ\text{C}$. A technique for determining the electrical properties of the investigated ceramics is proposed, which is based on an equivalent electric circuit allowing the recorded impedance spectra to be approximated with sufficiently high accuracy. The established spectral features are indicative of the presence of two electric relaxation times different from each other by three orders of magnitude. This fact is explained by the difference between the charge transport processes in the bulk of crystallites and thin intercrystallite spacers, for which the charge activation energies have been determined.

DOI: 10.1134/S1063783418020063

1. INTRODUCTION

At present, researchers take an active interest in high-temperature ceramics based on barium hexaaluminate $\text{BaO} \cdot 6\text{Al}_2\text{O}_3$ with isomorphic substitution of iron or manganese oxides for aluminum oxide, which leads to the occurrence of a number of new structural, mechanical, and electrical properties important for engineering applications [1]. These ceramics are used in fabrication of gas turbines due to their high refractory characteristics and, in addition, exhibit the catalytic properties of deep oxidation of a fuel during its high-temperature (up to 1700 K) combustion [2, 3]. On the other hand, these ceramics have an electrical conductivity and can therefore be used in high-temperature heating elements operating in air. In this case, the strong temperature dependence of the ceramics conductivity opens the opportunities for application in electronics, e.g., in heat resistors for automating of various high-temperature technological processes. Study of the electrical properties of ceramics is important not only for solving application tasks, but also for understanding the nature of specific features observed in these materials, including the high-temperature polarization and electric relaxation.

It is well known that the electrical conductivity of ceramic materials is caused by the ions located near

defects: in interstitial sites or near vacancies of the crystal lattice. Such ions can move from one defect to another and, in an electric field applied to the sample contacts, the electric current caused by the ion drift toward electrodes arises. If a ceramic material contains one-element ions of different valences, then the electrical conductivity can be caused by electrons hopping between these ions (electron hopping conductivity). This conductivity type is characteristic of a great number of ceramic materials, including the magnetically ordered compounds (ferrites) containing different-valence ions of $3d$ metals in the crystal lattice [4].

A specific feature of the studied barium hexaaluminate ceramics with four aluminum cations replaced by iron ($\text{BaO} \cdot 2\text{Fe}_2\text{O}_3 \cdot 4\text{Al}_2\text{O}_3$) is that iron ions are in the di- and trivalent states in the octahedral positions of the crystal lattice with a magnetoplumbite structure [3]. This facilitates electrons hopping between the localized ion states $\text{Fe}^{2+} \leftrightarrow \text{Fe}^{3+} + e^-$ and the occurrence of electron hopping conductivity. However, at this conductivity type, the spatial motion of electrons in ceramics can often be limited by various structural defects and potential barriers at the crystallite boundaries, including those on the intercrystallite spacers, where the charge accumulation regions can form. This leads to the occurrence of local electric fields directed

oppositely to the external electric field and to the spatially inhomogeneous (migration) polarization. The occurrence of the migration polarization is indicated by the anomalous growth of the real and imaginary permittivity components in the low-frequency range [5].

At present, there is a lack of detailed understanding of the electric polarization processes and nature of the conductivity in the ceramic materials based on barium hexaaluminate, because of insufficient experimental studies. They could be carried out, in particular, using impedance spectroscopy, which has been successfully used in studying the electrical properties of liquid crystals doped with an ion surfactant [6], electrode–liquid crystal interfaces [7], and electrical properties of thin magnetic films with a nanoisland structure [8]. Study of the impedance spectra are of special importance for the ceramic materials representing heterogeneous media with the complex composition and structure, the electrical properties of which originate from various processes of motion and accumulation of electric charges in both dc and ac electric fields.

Here we experimentally study the electrical properties of the barium hexaaluminate ceramics $\text{BaO} \cdot 2\text{Fe}_2\text{O}_3 \cdot 4\text{Al}_2\text{O}_3$ at different temperatures and frequencies to establish the correlation between electric charge transport and dielectric characteristics of this ceramics. The studies were carried out in the temperature range of 20–375°C at the electric field frequencies from 0.5 Hz to 100 MHz via measuring the impedance $Z = Z' - iZ''$ of a measuring cell in the form of a parallel-plate capacitor filled with the studied ceramics.

2. EXPERIMENTAL RESULTS

The studied ceramics was fabricated by hot pressing and sintering of the initial barium hexaaluminate prepared by the mechanochemical method described in [3]. In the initial material, four aluminum cations are replaced by iron ($\text{BaO} \cdot 2\text{Fe}_2\text{O}_3 \cdot 4\text{Al}_2\text{O}_3$). Measuring cells for experiments were fabricated in the form of parallel-plate capacitors containing plates $22.6 \times 8.4 \times 1.5$ mm in size cut from the obtained ceramics and metallized on their both sides by thermal vacuum deposition of chromium or nickel with a thickness of 0.5 μm onto polished plate surfaces. It is worth noting that the choice of a contact material is very important for recording the impedance spectra, since electric charge accumulation regions can form near electrodes [7] and induce additional migration polarization, thus masking the polarization and relaxation processes in the bulk of the studied material. The frequency dependences of the impedance of the fabricated samples were measured on an Agilent E5061B network analyzer at frequencies from 0.5 Hz to 100 MHz and temperatures from 20 to 375°C.

Figure 1 shows frequency dependences of the absolute value of the impedance $|Z|(f)$ and phase shift

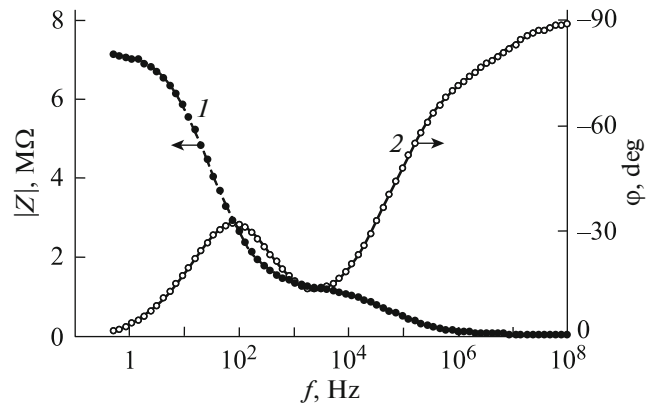


Fig. 1. Frequency dependence of the absolute value of the impedance $|Z|(f)$ (closed circles) and phase shift angle $\varphi(f)$ between the current and voltage (open circles) of a capacity cell with chromium electrodes on the $\text{BaO} \cdot 2\text{Fe}_2\text{O}_3 \cdot 4\text{Al}_2\text{O}_3$ ceramics.

angle $\varphi(f)$ between the current and voltage in a capacity measuring cell with the studied ceramics and chromium electrodes. The dependences were obtained at a temperature of $t = 20^\circ\text{C}$. It can be seen that the absolute value of the impedance of the studied ceramics (curve 1) in the low-frequency region ($f \sim 0.5$ Hz) attains its maximum value of $|Z| \sim 780$ k Ω , but, as the frequency increases to $f \sim 10^8$ Hz, the impedance drops by almost five orders of magnitude (to $|Z| \sim 20$ Ω). The phase-frequency response of the impedance (curve 2) has the pronounced minimum $\varphi_{\min} \sim -32^\circ$ at $f = 100$ Hz and maximum $\varphi_{\max} \sim -14^\circ$ at $f = 2.5$ kHz. With a further increase in the frequency, the phase shift tends to a value of $\varphi = -90^\circ$, which is indicative of a significant decrease in the loss in the capacity cell and of the almost complete disappearance of the conductivity contribution to the dielectric polarization of the studied ceramics. Note that the behavior of $|Z|(f)$ and $\varphi(f)$ for the sample measuring cell with nickel electrodes does not qualitatively differ from the dependences shown in Fig. 1.

The decrease in the conductivity contribution to the dielectric polarization of the ceramics at high frequencies is confirmed by the frequency dependence of the dissipation factor $\tan\delta(f)$ (inset in Fig. 2), which is determined as a ratio between the real impedance component $Z' = |Z|\cos\varphi$ and imaginary impedance component $Z'' = -|Z|\sin\varphi$. The frequency dependence of Z' is shown in Fig. 2 by closed circles (curve 1) and the frequency dependence of Z'' , by open circles (curve 2). In the $\tan\delta(f)$ dependence near $f = 2.5$ kHz, one can see the pronounced maximum attaining a value of $\tan\delta \sim 4$; however, with an increase in frequency, the dissipation factor rapidly decreases and at $f = 100$ MHz, it amounts to $\sim 10^{-2}$.

To interpret the electrical processes occurring in the studied ceramics in an ac electric field, it is conve-

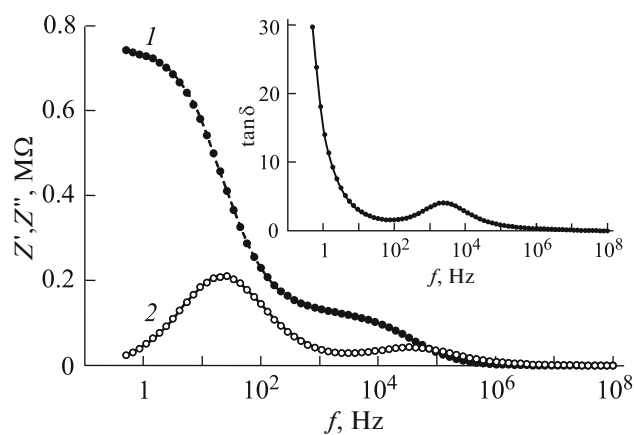


Fig. 2. Frequency dependences of the real (1) and imaginary (2) components of the impedance of the $\text{BaO} \cdot 2\text{Fe}_2\text{O}_3 \cdot 4\text{Al}_2\text{O}_3$ ceramics measured on a capacity cell with chromium electrodes. Inset: frequency dependence of the dissipation factor.

nient to analyze the measured spectra by presenting them in the form of a hodograph [6, 8], which is the dependence of the imaginary impedance component Z'' on the real component Z' (Fig. 3). It can be seen in Fig. 3 that the hodograph forms two contacting incomplete semi-circumferences, one (with a smaller diameter) starting nearly with the reference point and corresponding to the impedance spectrum in the high-frequency range and the other (with a larger diameter), corresponding to the impedance spectrum in the low-frequency range. Such a form of the hodograph indicates the existence of two different conductivity mechanisms in the studied ceramics, which can be demonstrated using the equivalent circuit shown in the inset in Fig. 3.

The equivalent circuit consists of two circuits connected in series, each being a resistor (active element) with a parallel reactive element ($R_{1,2}$ and $\text{CPE}_{1,2}$ in the circuit, respectively). These elements are included in the circuit because the centers of both the large and small semi-circumferences forming the hodograph in Fig. 3 are located below the ordinate axis, which is a typical sign of the existence of structural and electrical inhomogeneities in the studied substance, the properties of which are determined by the parts with the non-uniform active and reactive characteristics [9]. Selecting the nominals of elements of the equivalent circuit, we can approximate the points of the hodograph built on the basis of the measured impedance spectra with the required accuracy.

The nominals of the active elements of the equivalent circuit can be easily determined from the following considerations. At the frequency $f \rightarrow 0$, a point of intersection of the right-hand edge of the large semi-circumference with the abscissa axis corresponds to the static resistance of the studied sample: $Z' \equiv R_s \sim$

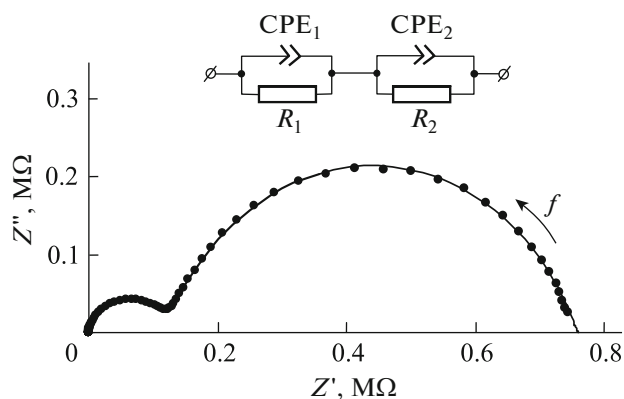


Fig. 3. Hodograph of the impedance of a capacity cell with chromium electrodes on the $\text{BaO} \cdot 2\text{Fe}_2\text{O}_3 \cdot 4\text{Al}_2\text{O}_3$ ceramics. Dots show the experiment and the solid line, the results of approximation with the use of the equivalent electric circuit.

$7.8 \times 10^5 \Omega$. Note that, taking into account the sample sizes, we can determine the resistivity of the studied ceramics: $\rho_s \sim 9.6 \times 10^4 \Omega \text{ m}$. Obviously, the resistance R_s is the sum of resistances R_1 and R_2 in the equivalent circuit (see the inset in Fig. 3). The resistance R_1 can be determined by extrapolation of the right-hand edge of the small semi-circumference arc of the hodograph in Fig. 3 to the intersection with the Z' axis ($R_1 \sim 1.7 \times 10^5 \Omega$). As a result, we have the resistance $R_2 = R_s - R_1 \sim 6.1 \times 10^5 \Omega$. Note that the two frequencies corresponding to the semi-circumference maxima in the hodograph are the frequencies of electric relaxation of two conductivity mechanisms: $f_1 \sim 3.3 \times 10^4 \text{ Hz}$ and $f_2 \sim 26.5 \text{ Hz}$. These frequencies allow us to determine the corresponding relaxation times: $\tau_1 \sim 4.8 \times 10^{-6} \text{ s}$ and $\tau_2 \sim 6.0 \times 10^{-3} \text{ s}$.

In determining the nominals of the reactive elements of the equivalent circuit, it is necessary to take into account the fact that the structure of ceramic materials is, as a rule, inhomogeneous due to the difference between sizes and orientations of crystallites separated by intercrystallite spacers. The crystallites are randomly distributed over a sample and form specific fractal conducting and polarization structures; the intercrystallite spacers in many ceramics are amorphous; however, they can also be partially crystallized. In such materials, the characteristics of reactive constant phase elements (CPEs) in the equivalent circuit is a universal tool for modeling the observed complex polarization phenomena related to charge accumulation and transport in a sample. For the studied ceramics, the CPE can be considered as a nonideal capacitor with the frequency-dependent capacitance and Q factor or as an element the characteristics of which correspond to the characteristics of a fragment of the fractal structure of a substance [10]. In this case, the CPE

Table 1. Parameters of elements of the equivalent circuit for $\text{BaO} \cdot 2\text{Fe}_2\text{O}_3 \cdot 4\text{Al}_2\text{O}_3$ ceramic capacity cells with chromium and nickel electrodes

Electrode material	Cr	Ni
R_1, Ω	1.7×10^5	2.2×10^5
R_2, Ω	6.1×10^5	1.8×10^6
η_1	0.76	0.85
η_2	0.75	0.72
$A_1, (\Omega^{-1} \text{s}^\eta)$	6.5×10^{-10}	1.6×10^{-10}
$A_2, (\Omega^{-1} \text{s}^\eta)$	3.7×10^{-8}	2.4×10^{-8}

impedance can be written in the form $Z_{\text{CPE}} = A^{-1}(i\omega)^{-\eta}$ [10], where A is the proportionality factor, i is the imaginary unit, and η is the index of fractal dimensionality of the structure. At $\eta = 1$, the CPE is a conventional capacitor and the coefficient A has a capacitance dimensionality. It is convenient to write the CPE complex impedance with the separated real and imaginary parts

$$Z_{\text{CPE}} = \frac{1}{A(i\omega)^\eta} = \frac{1}{A\omega^\eta} \left[\cos\left(\eta \frac{\pi}{2}\right) - i \sin\left(\eta \frac{\pi}{2}\right) \right]. \quad (1)$$

Obviously, for the electrical circuit consisting of two links connected in series (see the inset in Fig. 3), the total impedance $Z(\omega)$ is the sum of impedances of each link, $Z_1(\omega)$ and $Z_2(\omega)$

$$Z(\omega) = Z_1(\omega) + Z_2(\omega). \quad (2)$$

The impedances of each of two links of the equivalent circuit were calculated using the formula from [11], which was obtained with regard to (1):

$$Z_{1,2}(\omega) = R_{1,2} \frac{1 + A_{1,2}\omega^{\eta_{1,2}} R_{1,2} \left(\cos \frac{\eta_{1,2}\pi}{2} - i \sin \frac{\eta_{1,2}\pi}{2} \right)}{1 + R_{1,2}A_{1,2}\omega^{\eta_{1,2}} \left(R_{1,2}A_{1,2}\omega^{\eta_{1,2}} + 2 \cos \frac{\eta_{1,2}\pi}{2} \right)}. \quad (3)$$

The parameters of the reactive elements of the equivalent circuit were chosen to ensure the minimum deviation of the frequency dependence of its impedance from the corresponding characteristics measured of the experimental samples. Figure 3 (solid line) shows the results of approximation, which are in good agreement with the experimental data. This confirms the validity of using the two-link equivalent circuit for modeling the polarization and charge transport properties in the studied ceramics.

The optimal parameters of the equivalent circuit elements obtained for the studied $\text{BaO} \cdot 2\text{Fe}_2\text{O}_3 \cdot 4\text{Al}_2\text{O}_3$ ceramic samples with chromium and nickel electrodes are given in Table 1. It can be seen that the resistances R_1 and R_2 of the sample with nickel elec-

trodes are noticeably higher, which can be explained by the higher contact resistance of nickel electrodes and the measurement data obtained on the sample with chromium electrodes can therefore be considered to be more accurate. It is important that although the resistances R_1 and R_2 corresponding to the electrical resistances of crystallites and intercrystallite spacers slightly differ from each other, taking into account that the spacer thickness is significantly smaller than the crystallite size, we can state that the resistivity of the spacers is many times as large as the resistivity of crystallites. As a result, charges can be accumulated on these spacers between crystallites with the formation of a network of specific capacitors with high capacitance, which gives rise to the so-called migration polarization. This fact is confirmed by the CPE₂ capacitance coefficient A_2 of the intercrystallite spacers and exceeding the crystallite capacitance coefficient A_1 (Table 1).

As is known, the electrical properties of the studied ceramics strongly depend on temperature; in particular, upon heating of the ceramics, its electrical conductivity rapidly grows [3]. In addition, it is well known that, in the case of hopping conductivity, upon heating of the material the probability of overcoming the barriers by carriers increases; as a result, the resistance of the ceramics will exponentially decrease according to the Arrhenius law $R_s(T) = R_s \exp(E_a/k_B T)$, where E_a is the activation energy, T is the temperature (K), and k_B is the Boltzmann constant. To determine the activation energy, we measured frequency dependences of the impedance of the studied ceramics in the temperature range from 20 to 375°C, which were used to calculate the nominals of the corresponding elements of its electrical model (equivalent circuit).

Figure 4 shows temperature dependences of the resistances $R_1(t)$ and $R_2(t)$ of the electrical model of the ceramic sample with chromium electrodes. For the sake of convenience, we built the dependences on the reciprocal absolute temperature in logarithmic coordinates. It can be seen that the presented dependences contain two portions each, which are well approximated by straights. This confirms that the experimental temperature dependences of both the crystallite resistance $R_1(t)$ and intercrystallite spacer resistance $R_2(t)$ obey the Arrhenius law in each portion. In addition, it is important that the approximating straights intersect at the point $t_{c1} \sim 110^\circ\text{C}$ for the temperature dependence of the crystallite resistance and at the point $t_{c2} \sim 75^\circ\text{C}$ for the temperature dependence of the intercrystallite spacer resistance.

Obviously, using the Arrhenius law, we can easily determine activation energies for each portion of the temperature dependences from the slope of the approximating straights. It was found that these energies in the low-temperature portions are almost twice

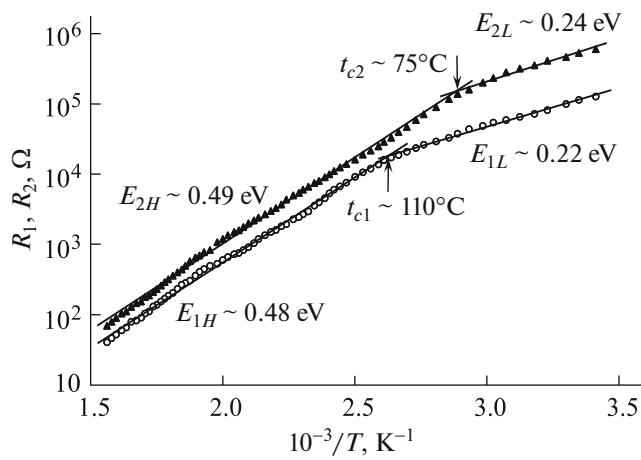


Fig. 4. Temperature dependence of resistances R_1 (closed symbols) and R_2 (open symbols) calculated from the impedance spectra for the equivalent circuit of a capacity cell filled with the $\text{BaO} \cdot 2\text{Fe}_2\text{O}_3 \cdot 4\text{Al}_2\text{O}_3$ ceramics. Straight lines show the approximation of the portions of the dependences by the Arrhenius law.

as low as in the high-temperature portions for both crystallites ($E_{1L} \sim 0.22$ eV and $E_{1H} \sim 0.48$ eV) and intercrystallite spacers ($E_{2L} \sim 0.24$ eV and $E_{2H} \sim 0.49$ eV) of the studied ceramics. Comparing the activation energies for crystallites and intercrystallite spacers, we can see that the difference between them in the low-temperature portions is smaller than 10%, while in the high-temperature portions, only 2%. Therefore, the hopping conductivity mechanism related to electrons hopping between localized states of ions $\text{Fe}^{2+} \rightarrow \text{Fe}^{3+} + e^-$ is implemented both in the bulk of crystallites and in the intercrystallite spacers.

Although the temperature dependences of the impedance strongly change with increasing temperature, they are still well approximated by the two-link electric circuit (see the inset in Fig. 3). This fact allowed us to determine temperature dependences of

Table 2. Parameters of elements of the equivalent circuit for a $\text{BaO} \cdot 2\text{Fe}_2\text{O}_3 \cdot 4\text{Al}_2\text{O}_3$ ceramic capacity cell with chromium electrodes obtained from the impedance spectra recorded at three temperatures

Sample temperature, °C	20	160	375
R_1, Ω	1.7×10^5	2.3×10^3	43
R_2, Ω	6.1×10^5	5.4×10^3	65
η_1	0.76	0.71	0.87
η_2	0.75	0.78	0.77
$A_1, (\Omega^{-1} \text{ s}^\eta)$	6.5×10^{-10}	3.3×10^{-9}	1.6×10^{-9}
$A_2, (\Omega^{-1} \text{ s}^\eta)$	3.7×10^{-8}	8.1×10^{-8}	1.9×10^{-7}

the nominals of the equivalent circuit, which are given in Table 2 for three temperatures corresponding to the boundaries of the studied temperature range and approximately to its middle point. It can be seen from Table 2 that upon heating the ceramics, we observe, along with a significant decrease in the resistances R_1 and R_2 , the significant increase in the capacitance coefficients A_1 and A_2 of CPEs in the equivalent circuit. This can be explained by the fact that with an increase in temperature, the probability of hopping of the electrons involved in the hopping conductivity of the ceramics grows, which facilitates the increase in the density of chargers accumulated on the crystallite and intercrystallite spacer boundaries. As expected, the fractality coefficients of the crystallite structure (η_1) and intercrystallite spacers (η_2) remain almost invariable with increasing temperature.

It is well known that the inhomogeneous polycrystalline structure of ceramic materials, which usually contains various defects, significantly affects not only the frequency dependences of the complex permittivity, but also the frequency dependences of the complex conductivity. The frequency dependences of the complex permittivity components $\epsilon'(\omega)$ and $\epsilon''(\omega)$ and complex conductivity components $\sigma'(\omega)$ and $\sigma''(\omega)$ can be easily calculated using the spectra of the real $Z'(\omega)$ and imaginary $Z''(\omega)$ components of the complex impedance of the measuring capacity cell (Fig. 2) filled with the studied material using the formulas [12, 13]

$$\epsilon'(\omega) = \frac{-Z''(\omega)d}{\epsilon_0\omega|Z(\omega)|^2 S}, \quad \epsilon''(\omega) = \frac{Z'(\omega)d}{\epsilon_0\omega|Z(\omega)|^2 S}, \quad (4)$$

and

$$\sigma'(\omega) = \frac{Z'(\omega) d}{|Z(\omega)|^2 S}, \quad \sigma''(\omega) = \frac{-Z''(\omega) d}{|Z(\omega)|^2 S}, \quad (5)$$

where d is the ceramic plate thickness, S is the measuring capacity cell contact area, and ϵ_0 is the permittivity of vacuum.

Figure 5 shows frequency dependences of the real and imaginary components of the permittivity (circles) and conductivity (triangles) calculated from formulas (4) and (5) from the impedance spectra recorded at a temperature of $t = 20^\circ\text{C}$. It can be seen that in the studied range of $0.5\text{--}10^8$ Hz, ϵ' decreases with increasing frequency by approximately three orders of magnitude and ϵ'' decrease by almost six orders of magnitude, while σ' increases by five orders of magnitude and σ'' almost doubles. Note that the observed features in the behavior of the presented dependences are apparently related to the features of charge polarizations and motion in the studied ceramics, which is confirmed, in particular, by the presence of two relaxation frequencies $f_1 \sim 3.3 \times 10^4$ Hz and $f_2 \sim 26.5$ Hz measured from the impedance hodograph (Fig. 3).

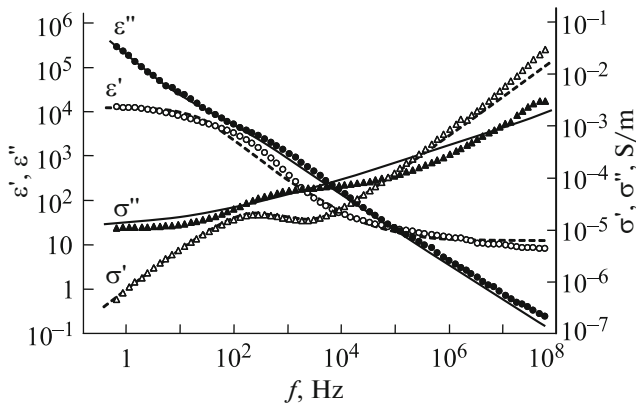


Fig. 5. Experimental dependences of the dispersion of complex permittivity components ϵ' and ϵ'' (circles) and complex conductivity components σ' and σ'' (triangles). Lines show the theoretical approximation of the corresponding dependences.

In addition, it should be noted that the relatively large values of the permittivity components observed in the low-frequency range are caused by the migration polarization of the ceramics due to the charge accumulation at the interfaces between crystallites and existing polycrystalline structure defects. In the high-frequency and microwave ranges, the migration polarization gradually disappears due to the high inertia of the processes of charge accumulation at the crystallite boundaries and on defects of the studied ceramics; in this frequency range, the permittivity is only caused by the polarization of the ceramics crystal structure.

As we mentioned above, crystallites in the studied ceramics form specific fractal conducting and polarization structures and, therefore, the theoretical approximation of the experimental frequency dependences of the real and imaginary permittivity components is most convenient to perform using the Cole–Cole model, in which the complex permittivity is described by the equation

$$\epsilon^*(\omega) = \epsilon_\infty + \frac{\epsilon_s - \epsilon_\infty}{1 + (j\omega\tau)^\alpha}. \quad (6)$$

Here, ϵ_s is the static permittivity, ϵ_∞ is the high-frequency (optical) permittivity, τ is the average permittivity relaxation time, and the parameter $0 < \alpha < 1$ characterizes the degree of the relaxation time spread around a certain average value. Using Eq. (6), we can easily obtain the expressions for the real (ϵ') and imaginary (ϵ'') permittivity components [14]. However, taking into account the fact that the studied ceramics is characterized by the complex conductivity, the imaginary permittivity component ϵ'' should be added

with a term that takes into account the frequency dependence of the conductivity

$$\epsilon'(\omega) = \epsilon_\infty + \frac{\left[1 + (\omega\tau)^\alpha \cos \frac{\alpha\pi}{2}\right](\epsilon_s - \epsilon_\infty)}{1 + 2(\omega\tau)^\alpha \cos \frac{\alpha\pi}{2} + (\omega\tau)^{2\alpha}} \quad (7)$$

and

$$\epsilon''(\omega) = \frac{(\epsilon_s - \epsilon_\infty)(\omega\tau)^\alpha \sin \frac{\alpha\pi}{2}}{1 + 2(\omega\tau)^\alpha \cos \frac{\alpha\pi}{2} + (\omega\tau)^{2\alpha}} + \frac{\sigma'(\omega)}{\epsilon_0\omega}. \quad (8)$$

It is important that there are several theories of hopping conductivity in materials with a complex (including fractal) structure; therefore, in modeling the frequency dependence of the conductivity, researchers usually choose the empirical models that take into account specific experimental conditions. For example, the frequency dependence of the real part of the hopping conductivity for a great number of compounds with variable valence is often described by a power equation like $\sigma'(\omega) = \sigma_{dc} + B\omega^n$, where σ_{dc} is the static conductivity, B is the proportionality factor, and $0 < n < 1$ is the exponent [5]. Sometimes, to obtain agreement with the experiment, more complex power dependences are used, e.g., $\sigma'(\omega) = B_1\omega^{n_1} + B_2\omega^{n_2}$ [15]. In our study, the best approximation of the experimental values presented in Fig. 5, was obtained using the relation [16]

$$\sigma'(\omega) = \sigma_{dc} \left[1 + \left(\frac{\omega}{\omega_H}\right)^n\right]. \quad (9)$$

Here, ω_H is the characteristic frequency of carrier hopping. The results of such an approximation of the real conductivity component $\sigma'(\omega)$ are shown in Fig. 5 by the solid line built at the following chosen constants: a static conductivity of the ceramics of $\sigma_{dc} = 1 \times 10^{-5} \Omega^{-1} \text{ m}^{-1}$, a characteristic hopping frequency of $\omega_H = 200 \text{ Hz}$, and $n = 0.35$. It can be seen that the theoretical dependence $\sigma'(\omega)$ built using formula (9) is in fairly good agreement with the experiment over almost the entire frequency range, but at the edge of the high-frequency range, there is some discrepancy.

The approximation of the measured $\epsilon'(\omega)$ and $\epsilon''(\omega)$ dependences using formulas (7) and (8), respectively, with regard to (9) is shown by dashed lines in Fig. 5 at the following chosen constants: $\epsilon_s = 1.3 \times 10^4$, $\epsilon_\infty = 9.8$, $\tau = 6 \times 10^{-3} \text{ s}$, and $\alpha = 0.78$. It can be seen that the theoretical dependences of the real (ϵ') and imaginary (ϵ'') permittivity components agree fairly well with the measured values over almost the entire frequency range. However, at the edge of the high-frequency range, there is a slight discrepancy between the theory and experiment for $\epsilon''(\omega)$, which is apparently related to the contribution of the real conductivity

component $\sigma'(\omega)$, the approximation of which using formula (9), as was mentioned above, somewhat differs from the experiment in the high-frequency range.

To theoretically approximate the frequency dependence of the imaginary component of the conductivity $\sigma''(\omega)$, we use formulas (4) and (5), which yield the expression

$$\sigma''(\omega) = \varepsilon_0 \varepsilon'(\omega) \omega. \quad (10)$$

Figure 5 (solid line) shows the $\sigma''(\omega)$ dependence built using formula (10), which is qualitatively consistent with the measurement data; however, it does not reflect the minor peculiarities in the behavior. This is explained by the simplicity of the model, where the $\sigma''(\omega)$ dispersion is determined by the dispersion of the effective capacitance of the measuring cell with a sample.

3. CONCLUSIONS

We studied the frequency and temperature dependences of the impedance of a measuring cell in the form of a parallel-plate capacitor filled with the barium hexaaluminate ceramics where four aluminum cations are replaced by iron ($\text{BaO} \cdot 2\text{Fe}_2\text{O}_3 \cdot 4\text{Al}_2\text{O}_3$). The measurements were performed in the frequency range of 0.5– 10^8 Hz at temperatures of 20–375°C. A technique for determining the electrical properties of the studied ceramics was proposed, which is based on an equivalent electric circuit allowing the recorded impedance spectra to be approximated with sufficient accuracy. Thus, we qualitatively estimated not only the electrical properties of the ceramics, but also the fractal dimensionality of its structure. The disclosed spectral features show the presence of two electric relaxation times, which differ from each other by three orders of magnitude. This fact is explained by the difference between the charge transport processes in the bulk of crystallites with the fractal structure and in thin intercrystallite spacers; for both, the charge activation energies were determined.

The dielectric properties of the ceramics were simulated using the Cole–Cole equation describing the dispersion properties of materials with a system of relaxors; the frequency dependence of the hopping conductivity was also taken into account using the empirical model from [16]. The models used describe fairly well the behavior of the complex permittivity and conductivity components of the ceramics in the studied frequency range. However, there is a noticeable deviation of the theoretical dependences from the measured ones starting from the edge of the high-fre-

quency range, which can be related to the occurrence of more complex electrical and dielectric relaxation processes in the studied ceramics. Therefore, to approximate the observed permittivity and conductivity dispersion in a wider frequency range, the Cole–Cole equation with the continuous distribution function of relaxation times may become necessary [17]. This function can be specified by modeling or determined numerically from the experimental dielectric spectra [18].

REFERENCES

1. M. Machida, K. Echuchi, and H. Arai, *Chem. Lett.*, 1993 (1986).
2. D. L. Trimm, *Appl. Catal.* **5**, 249 (1983).
3. V. A. Poluboyarov, O. V. Andryushkova, I. A. Pauli, and Z. A. Korotaeva, *Mechanical Effect on Physico-Chemical Processes in Solids* (Novosib. Gos. Tekh. Univ., Novosibirsk, 2011) [in Russian].
4. J. Smit and J. Wijn, *Ferrites* (Philips Technical Library, Eindhoven, 1959).
5. J. R. Macdonald, *J. Non-Cryst. Solids* **197**, 83 (1996).
6. B. A. Belyaev, N. A. Drokin, and A. N. Maslennikov, *Phys. Solid State* **56**, 1455 (2014).
7. B. A. Belyaev and N. A. Drokin, *Phys. Solid State* **57**, 181 (2015).
8. B. A. Belyaev and N. A. Drokin, *Phys. Solid State* **54**, 360 (2012).
9. E. Barsoukov and J. R. Macdonald, *Impedance Spectroscopy. Theory, Experiment, and Applications*, 2nd ed. (Wiley, New York, 2005).
10. N. G. Bukun and A. E. Ukshe, *Russ. J. Electrochem.* **45**, 11 (2009).
11. A. L. Zuev, V. Yu. Mishlanov, A. I. Sudakov, N. V. Shakhov, and A. V. Frolov, *Russ. Zh. Biomekh.* **16**, 110 (2012).
12. D. K. Pradhan, R. N. P. Choudhary, and B. K. Samantaray, *Int. J. Electrochem. Sci.* **3**, 597 (2008).
13. A. M. Solodukha and G. S. Grigoryan, *Vestn. Volgogr. Univ., Ser. Fiz. Mat.* **1**, 51 (2010).
14. V. V. Novikov and O. A. Komkova, *Tekhnol. Konstruir. Elektron. Appar.*, No. 5, 61 (2004).
15. R. Rizwana, T. Radha Krishna, A. R. James, and P. Sarah, *Cryst. Res. Technol.* **42**, 699 (2007).
16. S. Saha and T. P. Sinha, *Phys. Rev. B* **65**, 134103 (2002).
17. F. D. Morgan and D. P. Lesmes, *J. Chem. Phys.* **100**, 671 (1993).
18. B. A. Belyaev, N. A. Drokin, and V. F. Shabanov, *Phys. Solid State* **48**, 973 (2006).

Translated by E. Bondareva